Centrum voor Wiskunde en Informatica
Centre for Mathematics and Computer Science

H.T.M. van der Maarel, B. Koren

Spurious entropy generation in a non-smooth geometry

Department of Numerical Mathematics Report NM-R9009 May

The Centre for Mathematics and Computer Science is a research institute of the Stichting Mathematisch Centrum, which was founded on February 11, 1946, as a nonprofit institution aiming at the promotion of mathematics, computer science, and their applications. It is sponsored by the Dutch Government through the Netherlands Organization for the Advancement of Research (N.W.O.).

Spurious Entropy Generation in a Non-Smooth Geometry

Eric van der Maarel and Barry Koren
Centre for Mathematics and Computer Science
P.O. Box 4079, 1009 AB Amsterdam, The Netherlands

Numerical entropy generation is studied in the case of steady, subsonic Euler flow along a kinked solid wall. For a standard upwind finite volume discretization, the numerical entropy error appears to be zeroth-order in mesh size. Two possible causes of the zeroth-order entropy error are studied. First an investigation is made of the local discretization error on a kinked grid. Although this error also appears to be zeroth-order in the neighbourhood of the kink, it probably does not cause the zeroth-order entropy error. Next a study is made of the existence of a singularity in the exact solution. Probably, the Euler flow solution is singular at the kink in the wall. The form of this likely singularity is unknown. Therefore, the construction of a computational method which uses a priori knowledge about the singularity is not possible. Finally, it is shown by numerical experiment that the subsonic Euler flow along a kinked wall still can be computed with vanishing entropy errors, by using a continuously curved wall which converges to the kinked wall in the limit of zero mesh width.

1980 Mathematics Subject Classification: 35A40, 35B65, 35L65, 35L67, 65G99, 76N15.
Key Words & Phrases: steady Euler equations, subsonic flow, entropy error, discretization error, singularities.
Note: This work was supported by the European Space Agency (ESA), through Avions Marcel Dassault - Bréguet Aviation (AMD-BA).

1. Introduction

1.1. Outline

Numerical approximations of the subsonic Euler flow along a kinked solid wall show an erroneous entropy generation, which is virtually independent of the mesh size h of the computational grid. In this paper we study this numerical entropy generation for the steady, two-dimensional Euler equations. First we introduce the governing equations and the discretization method. Next, an example is given which shows the numerical accuracy of a subsonic Euler flow computation along a kinked wall. The solution clearly has a zeroth-order error in the entropy, one of the four solution components. In section 2, an investigation is made of the existing method's local discretization error and an improved discretization method is proposed. For supersonic flow on a kinked grid, the new discretization has no zeroth-order discretization errors. For subsonic flow, the new method has not that much practical value. In section 3, numerical results are given of the subsonic Euler flow along a kinked wall, using different types of grids. Despite the various improvements, all subsonic results still show a non-vanishing entropy error at the kink in the wall. Next, in section 4 the existence of a singularity in the solution of the continuous Euler equations is investigated, in relation to the error in the numerical approximation. A method is proposed for extracting a likely singularity from the solution. This method does not have much practical value either. Finally, in section 5 we show that it is yet still possible to approximately solve the Euler equations for the subsonic flow along a kinked wall with $O(h^{\mu})$-entropy errors, $0<\mu<1$, by approximating the kinked geometry with appropriate smooth geometries.

Report NM-R9009
Centre for Mathematics and Computer Science
P.O. Box 4079, 1009 AB Amsterdam, The Netherlands

1.2. Governing equations

The flow of an inviscid, non-heat conducting, perfect gas is described by the Euler equations and the perfect gas law. The unsteady, two-dimensional Euler equations can be written as

$$\frac{\partial \mathbf{q}}{\partial t}+\frac{\partial \mathbf{f}(\mathbf{q})}{\partial x}+\frac{\partial \mathbf{g}(\mathbf{q})}{\partial y}=\mathbf{0}, \tag{1}$$

with

$$\mathbf{q}=\begin{bmatrix}\rho\\ \rho u\\ \rho v\\ \rho E\end{bmatrix},\quad \mathbf{f}(\mathbf{q})=\begin{bmatrix}\rho u\\ \rho u^2+p\\ \rho uv\\ \rho uH\end{bmatrix},\quad \mathbf{g}(\mathbf{q})=\begin{bmatrix}\rho v\\ \rho uv\\ \rho v^2+p\\ \rho vH\end{bmatrix}. \tag{2}$$

In (2) the usual notations have been used: u and v for the velocity components in x- and y-direction, and ρ and p for the density and pressure. E denotes the total energy defined by $E=e+\frac{1}{2}(u^2+v^2)$, with e the internal energy, which for a perfect gas can be written as

$$e=\frac{1}{\gamma-1}\frac{p}{\rho}, \tag{3}$$

γ denoting the ratio of (constant) specific heats. For the total enthalpy H, defined by $H=E+p/\rho$, the Euler equations imply

$$\frac{DH}{Dt}\equiv\frac{\partial H}{\partial t}+u\frac{\partial H}{\partial x}+v\frac{\partial H}{\partial y}=\frac{1}{\rho}\frac{\partial p}{\partial t}. \tag{4}$$

In steady flow, this reduces to

$$u\frac{\partial H}{\partial x}+v\frac{\partial H}{\partial y}=0, \tag{5}$$

which means that along a streamline the total enthalpy is constant. Similarly, for the entropy, which for a perfect gas is defined by $s=p/\rho^{\gamma}$, the Euler equations imply

$$\frac{Ds}{Dt}=0. \tag{6}$$

This means that - except for possible discontinuities - entropy remains constant along a streamline.

1.3. Discretization

In this section we give a brief outline of the basic discretization method used in this paper: the upwind finite volume method which was first presented in [1]. The method has already shown to yield good numerical solutions and in many respects it can be considered as a good representative of a large class of upwind discretization methods. (See [2] for a comparison between the present basic discretization method and various other discretization methods.) Following Lax [3], we do not consider the steady Euler equations in differential form, but in the integral form which is found by integrating the steady version of (1) over some area Ω^*, some arbitrary subdomain of the computational domain Ω:

$$\iint_{\Omega^*}\left(\frac{\partial \mathbf{f}(\mathbf{q})}{\partial x}+\frac{\partial \mathbf{g}(\mathbf{q})}{\partial y}\right)dxdy=\oint_{\partial\Omega^*}(\mathbf{f}(\mathbf{q})n_x+\mathbf{g}(\mathbf{q})n_y)ds=\mathbf{0}. \tag{7}$$

In (7), $\partial\Omega^*$ is the boundary of Ω^*, and n_x and n_y are the x- and y-component of the outward unit normal at $\partial\Omega^*$. The Euler equations are then discretized by requiring (7) to hold for each $\Omega_{i,j}$, i.e. each i,j-th quadrilateral finite volume in a disjunct division of the computational domain Ω, $\bar{\Omega}=\bigcup_{i,j}\Omega_{i,j}$. Given a quadrilateral finite volume division, along $\partial\Omega_{i,j}$, the integral in (7) consists of four parts, each of which with constant n_x and n_y. At each cell face, the line integral is approximated by taking the

flux functions $\mathbf{f}(\mathbf{q})$ and $\mathbf{g}(\mathbf{q})$ constant and by computing them with Osher's numerical flux function [4], in the P-variant as proposed by Hemker and Spekreijse [1]. Denoting the cell face between e.g. $\Omega_{i,j}$ and $\Omega_{i+i,j}$ by $\partial\Omega_{i+\frac{1}{2},j}$ and the numerical flux functions approximating $\mathbf{f}(\mathbf{q})$ and $\mathbf{g}(\mathbf{q})$ by $\mathbf{F}(\mathbf{q}^l,\mathbf{q}^r)$ and $\mathbf{G}(\mathbf{q}^l,\mathbf{q}^r)$, the integral along cell face $\partial\Omega_{i+\frac{1}{2},j}$ can be written as

$$\int_{\partial\Omega_{i+\frac{1}{2},j}} (\mathbf{f}(\mathbf{q})n_x + \mathbf{g}(\mathbf{q})n_y)ds = \left[\mathbf{F}(\mathbf{q}^l_{i+\frac{1}{2},j},\mathbf{q}^r_{i+\frac{1}{2},j})(n_x)_{i+\frac{1}{2},j} + \mathbf{G}(\mathbf{q}^l_{i+\frac{1}{2},j},\mathbf{q}^r_{i+\frac{1}{2},j})(n_y)_{i+\frac{1}{2},j} + \mathbf{O}(h^\mu)\right] l_{i+\frac{1}{2},j}, \quad (8)$$

where $l_{i+\frac{1}{2},j}$ is the length of $\partial\Omega_{i+\frac{1}{2},j}$, $(n_x)_{i+\frac{1}{2},j}$ and $(n_y)_{i+\frac{1}{2},j}$ the components of the outward unit normal at $\partial\Omega_{i+\frac{1}{2},j}$, $\mathbf{q}^l_{i+\frac{1}{2},j}$ and $\mathbf{q}^r_{i+\frac{1}{2},j}$ the states at the left and right side of $\partial\Omega_{i+\frac{1}{2},j}$ and μ the order of accuracy of the approximation. In this paper, we take the state vector $\mathbf{q}_{i,j}$ constant over each cell $\Omega_{i,j}$, so the left and right states at e.g. cell face $\partial\Omega_{i+\frac{1}{2},j}$ are

$$\begin{aligned} \mathbf{q}^l_{i+\frac{1}{2},j} &= \mathbf{q}_{i,j}, \\ \mathbf{q}^r_{i+\frac{1}{2},j} &= \mathbf{q}_{i+1,j}. \end{aligned} \quad (9)$$

On a smooth grid, the use of these piecewise constant state vectors in a finite volume leads to a first-order accurate discretization, $\mu = 1$.

Boundary conditions are incorporated into the scheme in a way which is consistent with the discretization in the interior of the computational domain. In subsonic flows, this requires that *three* boundary conditions are imposed at inflow and *one* boundary condition at outflow. (We remark that by just obeying these numbers in subsonic flow computations, mathematical well-posedness is not yet guaranteed. For a study of the mathematical well-posedness of e.g. some typical subsonic outlet boundary conditions, we refer to [5].) For supersonic flow, the number of boundary conditions to be imposed at in- and outflow is *four* and *zero*, respectively.

In this paper we will mainly consider flows of which the *exact* solutions are known to be homentropic. We will make proper use of this knowledge to monitor the quality of *numerical* solutions obtained for these flows. As already mentioned in section 1.2, in steady subsonic flow the entropy along a streamline is constant. Hence, a first requirement for obtaining a homentropic flow in a numerical computation is to impose a constant entropy at inflow.

1.4. The problem

In the following we study the entropy errors for a subsonic Euler flow along a kinked wall (Figure 1). At the inflow boundary, the velocity vector and the entropy are imposed. The imposed velocity corresponds with that of an incompressible, irrotational flow along a kinked wall. At outflow, the corresponding pressure is imposed.

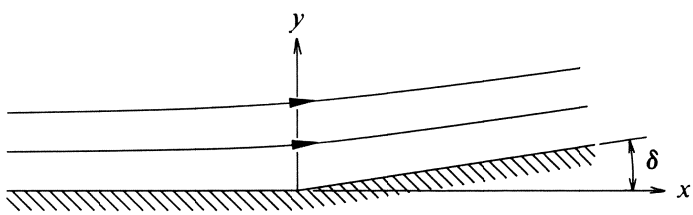

Figure 1. Kinked wall.

The type of grid used is shown in Figure 2. It consists of 32×32 finite volumes. Coarser grids (16×16 and 8×8) are obtained from the finer by leaving out each second mesh line. Entropy errors obtained are shown in Figure 3. The results show that the entropy error is virtually independent of the mesh size, they clearly outline the problem to be studied in this paper. (We emphasize that the entropy variation can be seen as a monitor for the error in *all* solution components. Most likely, the other solution components will also have zeroth-order errors.) Possible causes of the zeroth-order error behaviour are:

(i) an excessive non-smoothness of the grid (The grid used is non-smooth along the entire grid line emerging from the kink in the wall.), or

(ii) a singularity in the exact solution of the continuous equations, at the kink in the wall. (For $\delta\in(0,\pi/2)$, δ denoting the kink angle, see Figure 1, the incompressible potential flow along that wall has a singularity in the velocity field, which is of the form $r^{\delta/(\pi-\delta)}$, r denoting the radial distance from the kink. The subsonic Euler flow along a kinked wall may well have a similar singularity.)

In the following sections, these two possible causes will be investigated, in order to understand what causes the zeroth-order error behaviour, and - if possible - to improve the accuracy of the approximation.

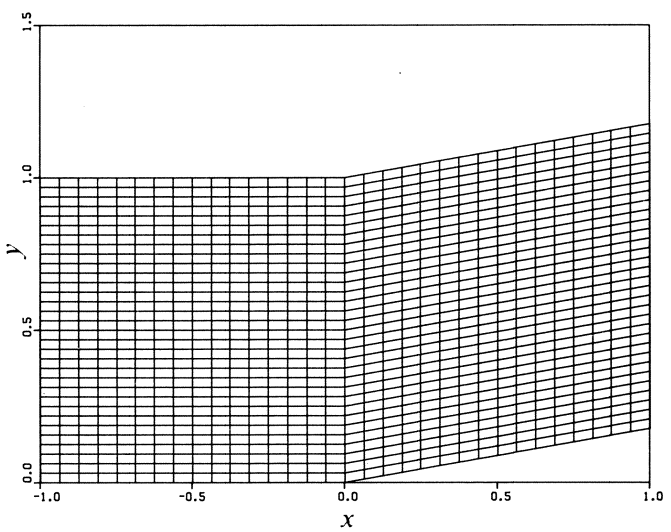

Figure 2. Kinked grid, 32×32.

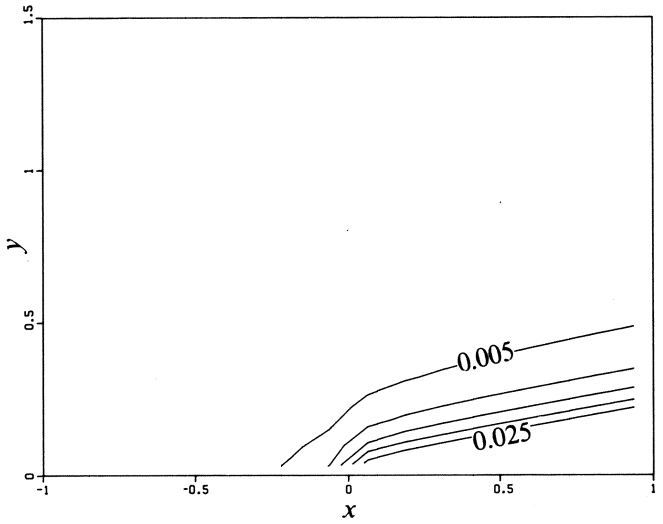

a. Iso-plot entropy error, 16×16-grid.

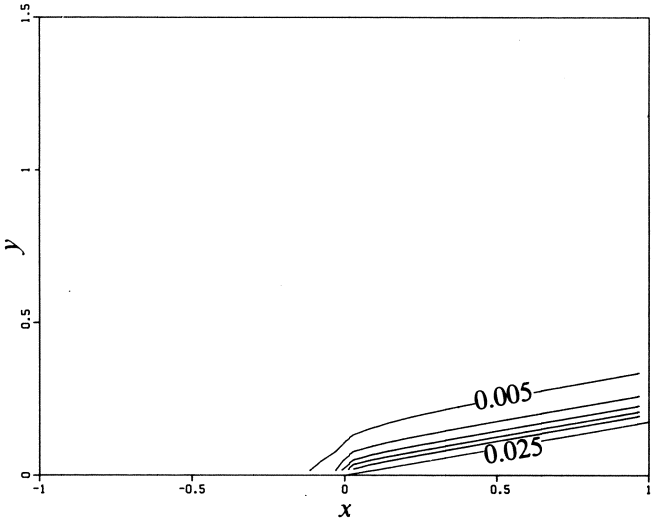

b. Iso-plot entropy error, 32×32-grid.

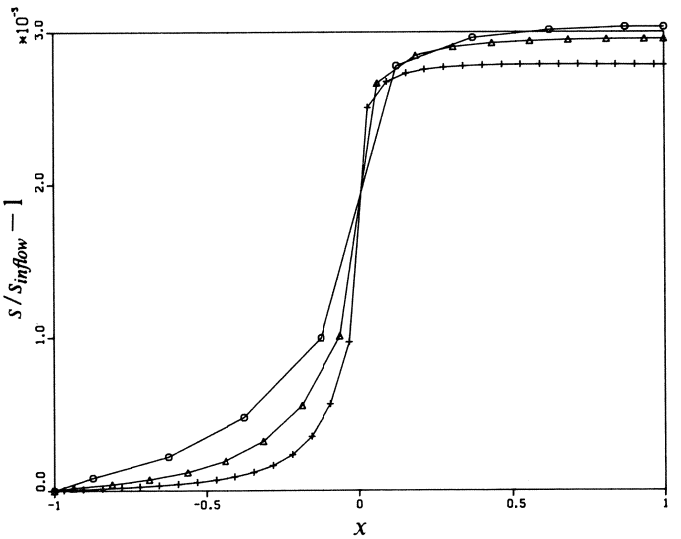

c. Entropy error along kinked wall,
○:8×8-grid, Δ:16×16-grid, +:32×32-grid.

Figure 3. Entropy error distributions, kinked grid, $\delta = 10°$.

2. Non-smoothness of the grid

Having noticed the zeroth-order behaviour of the entropy error, it is natural first to investigate the discretization error of the numerical scheme. In the following we study the effect of the grid non-smoothness on the local discretization error of the upwind finite volume discretization.

2.1. Local discretization error

In section 1.3 we mentioned that the flux functions at e.g. cell face $\partial\Omega_{i+\frac{1}{2},j}$ are approximated by

$$\begin{aligned}(\mathbf{f}(\mathbf{q}))_{i+\frac{1}{2},j} &= \mathbf{F}(\mathbf{q}_{i,j},\mathbf{q}_{i+1,j})+\mathbf{O}(h),\\ (\mathbf{g}(\mathbf{q}))_{i+\frac{1}{2},j} &= \mathbf{G}(\mathbf{q}_{i,j},\mathbf{q}_{i+1,j})+\mathbf{O}(h).\end{aligned} \tag{10}$$

Let $\mathbf{q}$ denote the exact, continuous solution of the Euler equations in the domain covered by the grid as shown in Figure 2 and let $\mathbf{q}_{i,j}$ denote the discrete value of $\mathbf{q}$ in the centre of $\Omega_{i,j}$. Then, for $\Omega_{i*,j}$, a cell just behind the kink in the grid (Figure 4), the system of discretized equation reads

$$\begin{aligned}&\left[\mathbf{F}(\mathbf{q}_{i*,j},\mathbf{q}_{i*+1,j})-\mathbf{F}(\mathbf{q}_{i*-1,j},\mathbf{q}_{i*,j})\right]\\ &+2\tan\delta\left[\mathbf{F}(\mathbf{q}_{i*,j-1},\mathbf{q}_{i*,j})-\mathbf{F}(\mathbf{q}_{i*,j},\mathbf{q}_{i*,j+1})\right]\\ &+2\left[\mathbf{G}(\mathbf{q}_{i*,j},\mathbf{q}_{i*,j+1})-\mathbf{G}(\mathbf{q}_{i*,j-1},\mathbf{q}_{i*,j})\right]=\mathbf{0}.\end{aligned} \tag{11}$$

Taylor series expansion around the centre of $\Omega_{i*,j}$ yields for the first term in (11):

$$\mathbf{F}(\mathbf{q}_{i*,j},\mathbf{q}_{i*+1,j})=\mathbf{F}(\mathbf{q}_{i*,j},\mathbf{q}_{i*,j})+2h\left[\frac{\partial\mathbf{F}(\mathbf{q}_{i*,j},\mathbf{q})}{\partial\mathbf{q}}\frac{\partial\mathbf{q}}{\partial x}\right]\Bigg|_{i*,j}+2h\tan\delta\left[\frac{\partial\mathbf{F}(\mathbf{q}_{i*,j},\mathbf{q})}{\partial\mathbf{q}}\frac{\partial\mathbf{q}}{\partial y}\right]\Bigg|_{i*,j}. \tag{12}$$

Similar formulae for the other terms in (11) and

$$\frac{\partial\mathbf{F}}{\partial x}\Bigg|_{i,j}=\left[\frac{\partial\mathbf{F}(\mathbf{q},\mathbf{q}_{i,j})}{\partial\mathbf{q}}\frac{\partial\mathbf{q}}{\partial x}\right]\Bigg|_{i,j}+\left[\frac{\partial\mathbf{F}(\mathbf{q}_{i,j},\mathbf{q})}{\partial\mathbf{q}}\frac{\partial\mathbf{q}}{\partial x}\right]\Bigg|_{i,j}, \tag{13}$$

then yield as modified equation for (11):

$$\frac{\partial\mathbf{F}}{\partial x}\Bigg|_{i*,j}+\frac{\partial\mathbf{G}}{\partial y}\Bigg|_{i*,j}-\frac{1}{2}\tan\delta\left[\frac{\partial\mathbf{F}(\mathbf{q},\mathbf{q}_{i*,j})}{\partial\mathbf{q}}\frac{\partial\mathbf{q}}{\partial y}\right]\Bigg|_{i*,j}=\mathbf{O}(h). \tag{14}$$

From (14), we see that the discretization has a zeroth-order error. The error vanishes for $\delta=0$ (of course), or for fully one-sided upwind discretization from the right. (In the latter case $\mathbf{F}(\mathbf{q},\mathbf{q}_{i*,j})=\mathbf{f}(\mathbf{q}_{i*,j})$ and hence $\partial\mathbf{F}(\mathbf{q},\mathbf{q}_{i*,j})/\partial\mathbf{q}=\mathbf{0}$.) A similar result is obtained when we analyze the local discretization error for a cell $\Omega_{i*-1,j}$ just in front of the kink:

$$\frac{\partial\mathbf{F}}{\partial x}\Bigg|_{i*-1,j}+\frac{\partial\mathbf{G}}{\partial y}\Bigg|_{i*-1,j}+\frac{1}{2}\tan\delta\left[\frac{\partial\mathbf{F}(\mathbf{q}_{i*-1,j},\mathbf{q})}{\partial\mathbf{q}}\frac{\partial\mathbf{q}}{\partial y}\right]\Bigg|_{i*-1,j}=\mathbf{O}(h). \tag{15}$$

So, for a cell just in front of the kink the zeroth-order error vanishes for a fully *left*-sided upwind discretization, or - of course - for vanishing δ.

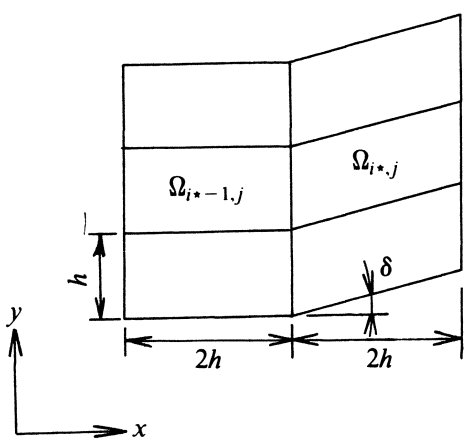

Figure 4. Geometry at kink.

To verify the analysis, we compute the residual of an exact solution of the Euler equations, by substituting this solution into the discretized equations. For the exact solution we take a supersonic, non-uniform, parallel flow

$$(u,v,\rho,p)^T=(u_0+u_1y,0,\rho_0,p_0)^T, \tag{16}$$

with u_0, u_1, ρ_0, p_0 constant, u_0 and u_1 both positive. No solid wall boundary is involved in this flow. Since the flow solution has a gradient in y-direction, for $\delta\neq 0$ we expect to find a zeroth-order discretization error. Since the flow is supersonic from the left, we should find zeroth-order residuals only in cells just behind the kink. Numerical results show that zeroth-order errors are concentrated around the cell centres just behind the kink indeed (Figure 5). If we take the same supersonic flow in the opposite direction ($u_0<0$, $u_1<0$), zeroth-order residuals are concentrated around cell centres just in front of the kink (Figure 6a). In subsonic flow (Figure 6b), we find zeroth-order residuals both in front and behind the kink, as could be expected from (14) and (15), since in subsonic flow the numerical flux function depends on both the left and right state. (As can be seen from both Figure 5 and 6, along a part of the boundary, zeroth-order discretization errors are found as well. Apparently, the boundary of the computational domain introduces local discretization errors as though the grid were kinked at the boundary. It can be proved that at the boundary, the behaviour of the discretization error with respect to the upwind direction, is identical indeed to that at the kink in the grid.)

REMARK. The residuals presented in Figure 5 and 6 are those of the Euler equations discretized by a finite volume method and hence they are integrated quantities. In order to compare residual fields of such a discretization on a family of grids, they have to be scaled with their corresponding volume areas; therefore, in both figures we have given the iso-levels of $\int\int_{\Omega_{i,j}}(\text{residual})dxdy / \int\int_{\Omega_{i,j}}dxdy$.

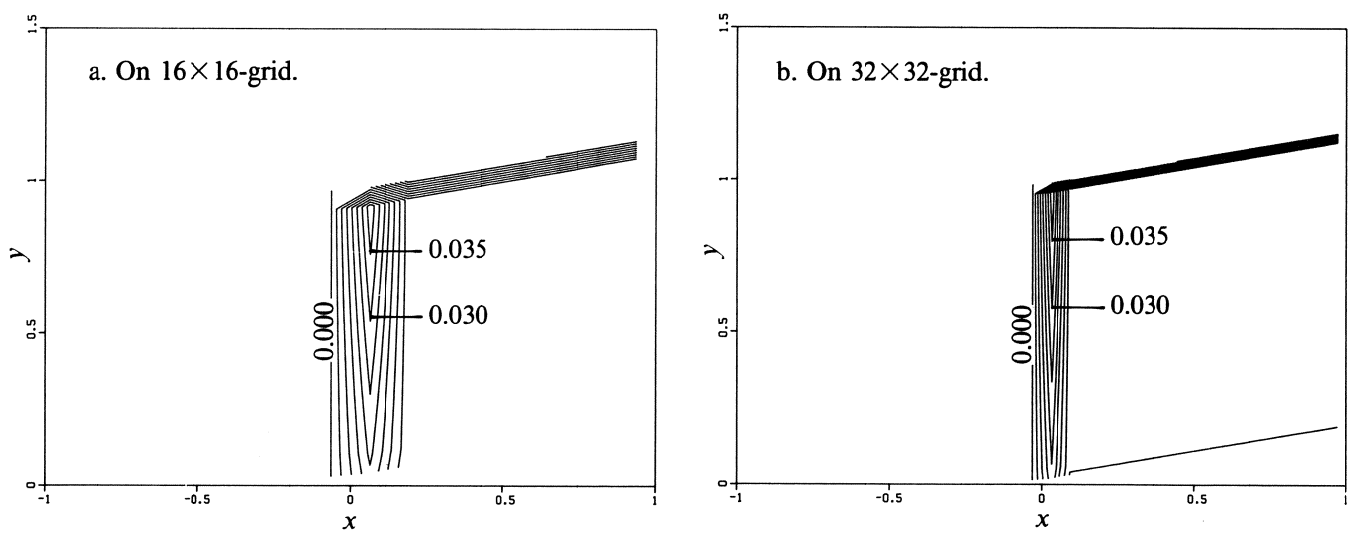

Figure 5. Iso-plots residual energy equation, supersonic flow from the left, $\delta=10^o$ (without wall).

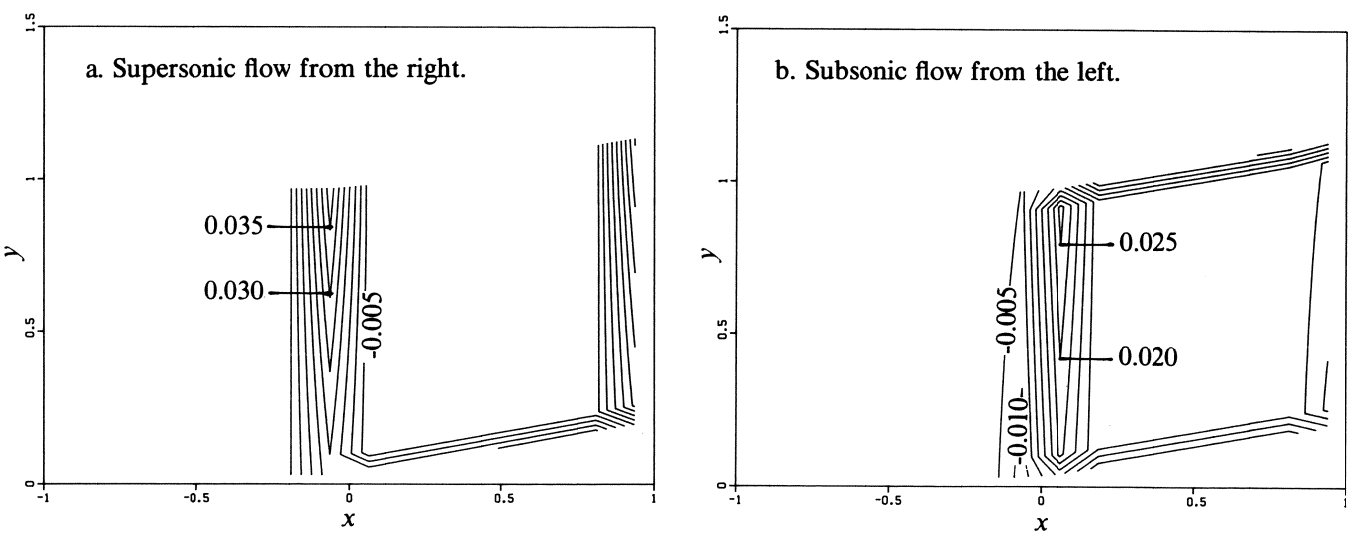

Figure 6. Iso-plots residual energy equation, 16×16-grid, $\delta=10^o$ (without wall).

2.2. New discretization

The zeroth-order discretization errors as derived in section 2.1, only involve derivatives in y-direction, i.e. the direction in which the cells behind the kink are shifted. In this section we try to remove these errors by enlarging the stencil of the discretization. Since for this purpose, we only need to introduce extra derivatives in y-direction, we simply extend the stencil in y-direction. We introduce a *new* flux across $\partial\Omega_{i*+\frac{1}{2},j}$, by taking a weighted mean of the *existing* numerical fluxes across $\partial\Omega_{i*+\frac{1}{2},j}$ and $\Omega_{i*+\frac{1}{2},j+1}$, i.e. we approximate $\mathbf{f}_{i*+\frac{1}{2},j}$ by

$$\mathbf{f}_{i*+\frac{1}{2},j}=a_{i*+\frac{1}{2},j}\mathbf{F}(\mathbf{q}_{i*,j},\mathbf{q}_{i*+1,j})+(1-a_{i*+\frac{1}{2},j})\mathbf{F}(\mathbf{q}_{i*,j+1},\mathbf{q}_{i*+1,j+1}). \tag{17}$$

The same is done for the approximation of the flux across $\partial\Omega_{i*-\frac{1}{2},j}$:

$$\mathbf{f}_{i*-\frac{1}{2},j}=a_{i*-\frac{1}{2},j}\mathbf{F}(\mathbf{q}_{i*-1,j},\mathbf{q}_{i*,j})+(1-a_{i*-\frac{1}{2},j})\mathbf{F}(\mathbf{q}_{i*-1,j+1},\mathbf{q}_{i*,j+1}). \tag{18}$$

Substitution of (17) and (18) into the discrete version of (7) and Taylor series expansion around the centre of $\Omega_{i*,j}$, then yields as modified equation

$$\frac{\partial\mathbf{F}}{\partial x}\bigg|_{i*,j}+\frac{\partial\mathbf{G}}{\partial y}\bigg|_{i*,j}+\frac{1}{2}(a_{i*-\frac{1}{2},j}-a_{i*+\frac{1}{2},j}-\tan\delta)\frac{\partial\mathbf{F}}{\partial y}\bigg|_{i*,j}+\frac{1}{2}\tan\delta\left[\frac{\partial\mathbf{F}(\mathbf{q}_{i*,j},\mathbf{q})}{\partial\mathbf{q}}\frac{\partial\mathbf{q}}{\partial y}\right]\bigg|_{i*,j}=\mathbf{O}(h). \tag{19}$$

In a fully one-sided upwind discretization from the left (i.e. in a supersonic flow with $u>0$), the fourth term in (19) is equal to zero by itself. The third term can be made equal to zero by choosing the weights such that they satisfy $a_{i*-\frac{1}{2},j}-a_{i*+\frac{1}{2},j}-\tan\delta=0$. So applying this new discretization to (16), in the case of supersonic flow from the left, the fourth term in (19) drops automatically. Using the old discretization for that flow, there was no zeroth-order discretization error in $\Omega_{i*-1,j}$ (see Figure 5). To ensure that there is still no zeroth-order discretization error in $\Omega_{i*-1,j}$, in that volume we still use the old discretization (i.e. $a_{i*-\frac{1}{2},j}=1$). Hence, by choosing

$$\begin{aligned} a_{i*-\frac{1}{2},j}&=1,\\ a_{i*+\frac{1}{2},j}&=1-\tan\delta, \end{aligned} \tag{20}$$

the zeroth-order error in $\Omega_{i*,j}$ should vanish for supersonic flow from the left, without introducing a zeroth-order error in $\Omega_{i*-1,j}$. However, this new discretization for $i=i*$ does introduce zeroth-order errors in the cells downstream of $\Omega_{i*,j}$. In order to remove these errors, we apply the new discretization in all cells downstream of the kink. In Figure 7 now, local discretization errors are given, as found by substitution of the exact solution (16) into the new system of discretized equations. We observe that the error is first-order indeed.

In subsonic flow, the Riemann solver is not fully one-sided and as a consequence, in subsonic flow the zeroth-order local discretization error in (19) can be removed only by making the *sum* of the third and fourth term in (19) equal to zero. In that case the weights $a_{i*-\frac{1}{2},j}$ and $a_{i*+\frac{1}{2},j}$ become dependent of the solution. So, in subsonic flow the zeroth-order local discretization error cannot be removed without introducing a significantly more complicated discretization. Before making any attempt to construct a discretization of this kind, we will first investigate to what extent the zeroth-order discretization error actually causes the zeroth-order solution error.

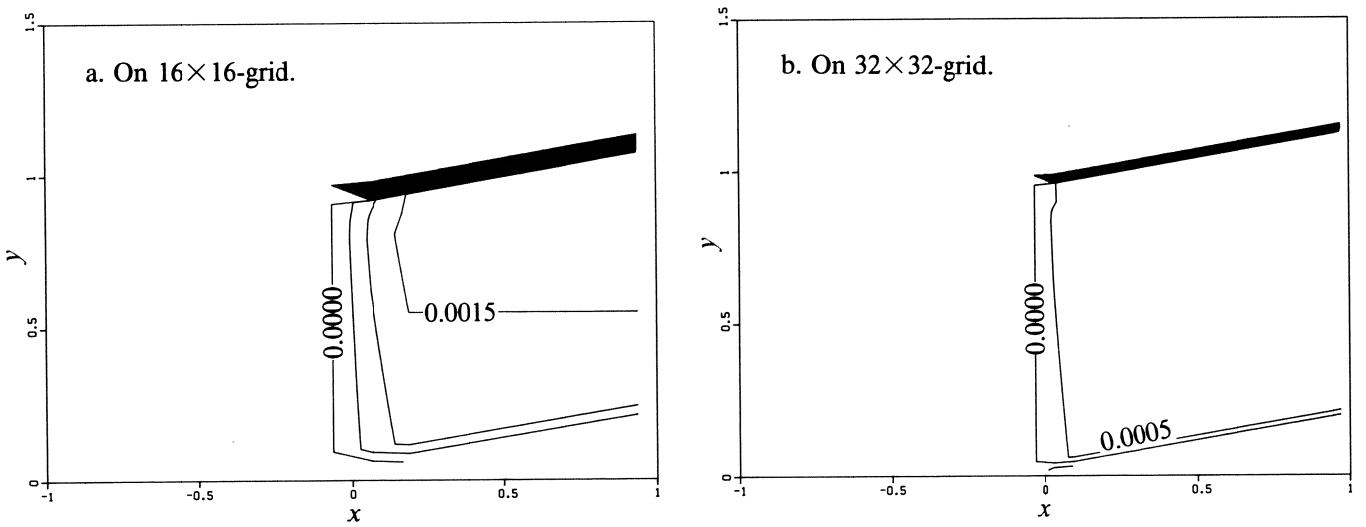

Figure 7. Iso-plots residual energy equation, supersonic flow from the left, $\delta=10^{o}$ (without wall), new discretization.

2.3. Entropy error on a kinked grid not involving a wall

In this section we study the *entropy* error on a kinked grid without wall. The purpose is to find out whether or not the zeroth-order entropy error, as found in the approximation of the flow along a kinked wall (Figure 3), is caused by the zeroth-order local discretization error on a kinked grid. We consider the old discretization and a subsonic version of (16) as the exact flow field. Yet we will not use this exact flow field to obtain the discretization error, but to *solve* the discretized equations by imposing it via the boundary conditions. If for the flow without wall, on the kinked grid shown in Figure 2, zeroth-order errors in the solution field are found, then they may be caused by the zeroth-order local discretization error. However, if we do *not* find zeroth-order errors in the approximate solution, assuming that the parallel flow considered is not too trivial, the kinked grid and the resulting zeroth-order discretization errors do *not* introduce zeroth-order errors in the solution field.

Results are given in Figure 8, which shows the entropy error in the bottom row of cells, for different mesh sizes. The results clearly show that the entropy error becomes approximately twice as small when the mesh size is made twice as small. This first-order entropy behaviour seems to imply that the zeroth-order local discretization error which was found on the kinked grid, is harmless indeed. Therefore, we postulate that the zeroth-order entropy error as found in the approximation of the subsonic flow along a kinked wall is *not* caused by the zeroth-order local discretization error.

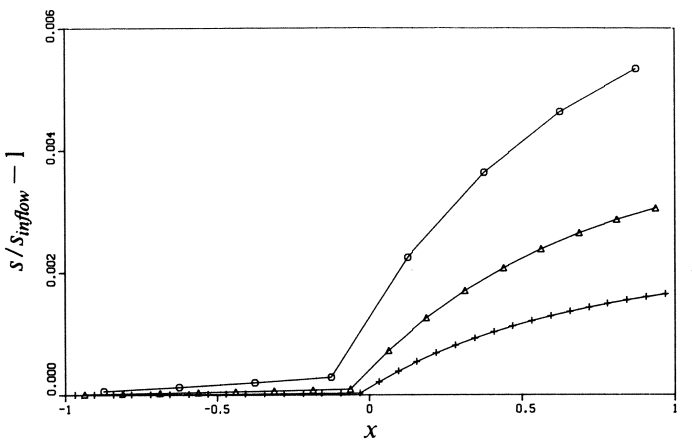

Figure 8. Entropy error in bottom row of cells, subsonic flow from the left, $\delta = 10^{o}$ (without wall), old discretization, $\bigcirc$:8×8-grid, Δ:16×16-grid, +:32×32-grid.

3. Entropy errors in a slightly different situation

3.1. Entropy error along a smooth wall

In this section we study the entropy error in the flow along a continuously curved wall. This is done, in order to make sure that the solid wall boundary condition, or rather its implementation, is not the cause of the zeroth-order entropy error. The shape of the wall which we will use, is given by

$$y_w(x) = \begin{cases} 0, & x \leqslant -\tfrac{1}{2}l, \\ \tan\delta \dfrac{(x+\tfrac{1}{2}l)^3}{l^2} - \tfrac{1}{2}\tan\delta \dfrac{(x+\tfrac{1}{2}l)^4}{l^3}, & -\tfrac{1}{2}l < x \leqslant \tfrac{1}{2}l, \\ \tan\delta\, x, & x > \tfrac{1}{2}l. \end{cases} \tag{21}$$

Here, l is the length of the curved part of the wall (Figure 9) and δ the angle between the positive x-direction and the uncurved part of the wall at $x \geqslant \tfrac{1}{2}l$ (Figure 9). The wall is defined in such a way that $y_w(x)$ is a C^2-function. The type of grid used is shown in Figure 10. In Figure 11, for $l=1$ and three mesh sizes, the entropy error along the wall is given. We see that the entropy error is first-order in mesh size. Since the scheme is first-order on smooth grids, this is what we were expecting. So, for sake of clearness we have shown here that no zeroth-order entropy errors are introduced by the solid wall boundary condition treatment.

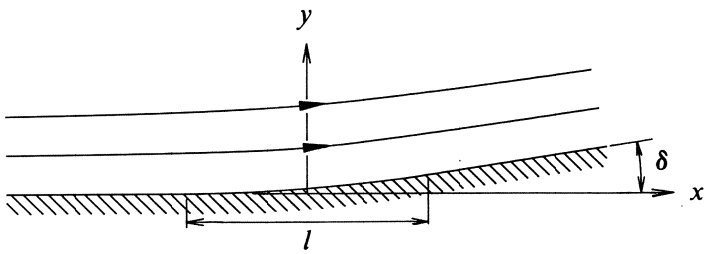

Figure 9. Continuously curved wall.

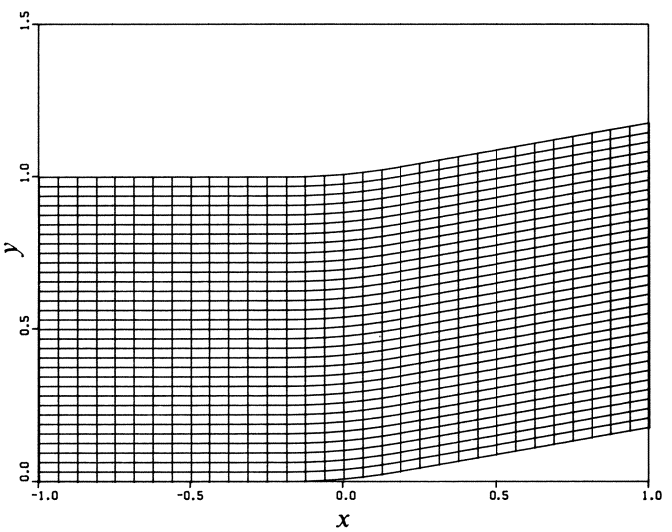

Figure 10. Continuously curved grid, 32×32.

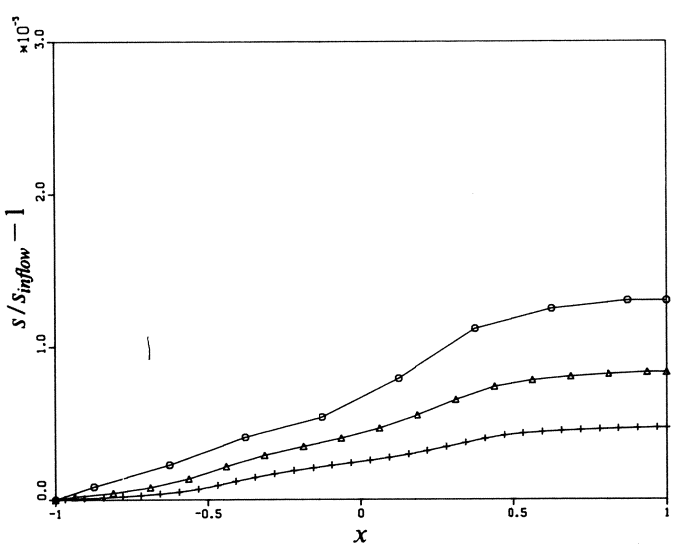

Figure 11. Entropy error along continuously curved wall, $\delta = 10°$, ○:8×8-grid, Δ:16×16-grid, +:32×32-grid.

3.2. Entropy error for other types of grids

In this section we study the entropy error when the Euler flow along the kinked wall is approximated on two types of grids which are essentially different from the simple kinked grid (Figure 2) as applied in the previous sections. First a grid is used which is only kinked at the wall (Figure 12a). In the interior of the domain it is smooth and orthogonal, its grid lines are hyperboles. We will call this grid the hyperbolic grid. Since this grid is smooth, except at a single point, it will not cause zeroth-order local discretization errors along the $i\star$-th grid line, as does the simple kinked grid. The other grid, shown in Figure 12b, does not contain any kink at all, but it has degenerated quadrilaterals located at the kink. We call this grid the circular grid. Entropy errors along the wall, as obtained on these grids are shown in Figure 13. For both grids we immediately see that the entropy error is also zeroth-order at the kink. This is also shown in Figure 14 and 15. However, from the latter figures it also appears that at a small, fixed distance away from the wall, the entropy error becomes first-order. A peculiarity of the results obtained on the circular grid, in comparison to those obtained on the hyperbolic and kinked grid, is that the entropy error along the wall decreases after the kink. We think that this phenomenon, which we already know from airfoil flow computations (see e.g. [6]), is mainly caused by a greater amount of crosswise numerical diffusion on the circular grid. Another cause may be the fact that for the circular grid, in streamwise direction behind the kink, the cell sizes increase. As a consequence, the first-order interpolation from a cell centre towards the wall (as applied in the present boundary condition treatment [1]) becomes worse, which may (also) contribute to the entropy decrease along the wall.

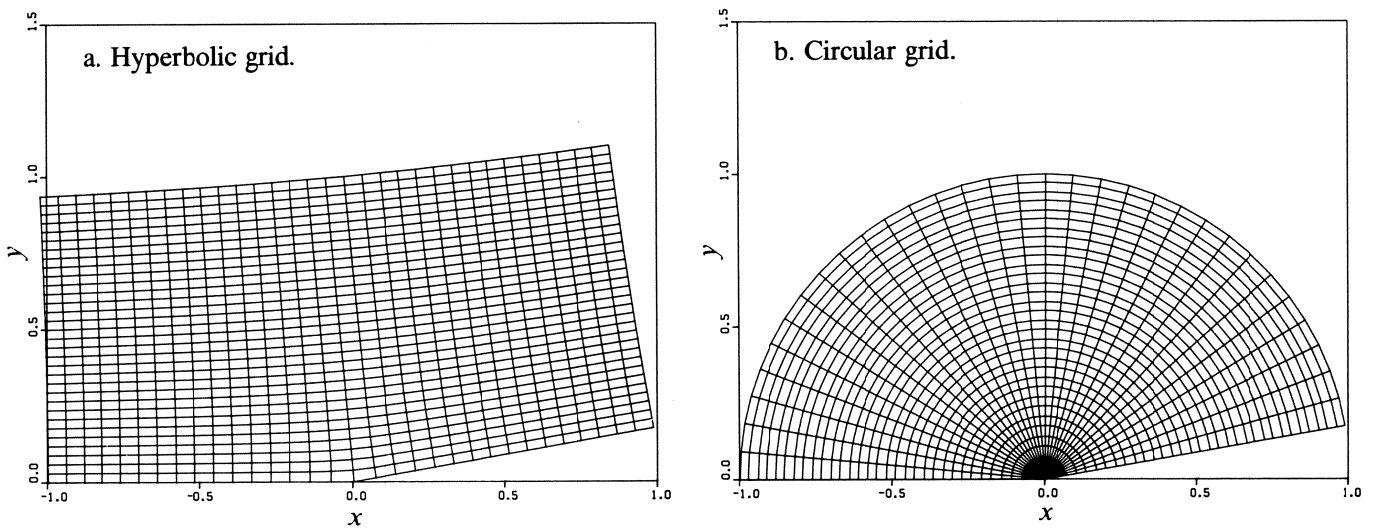

Figure 12. Other types of grids, 32×32.

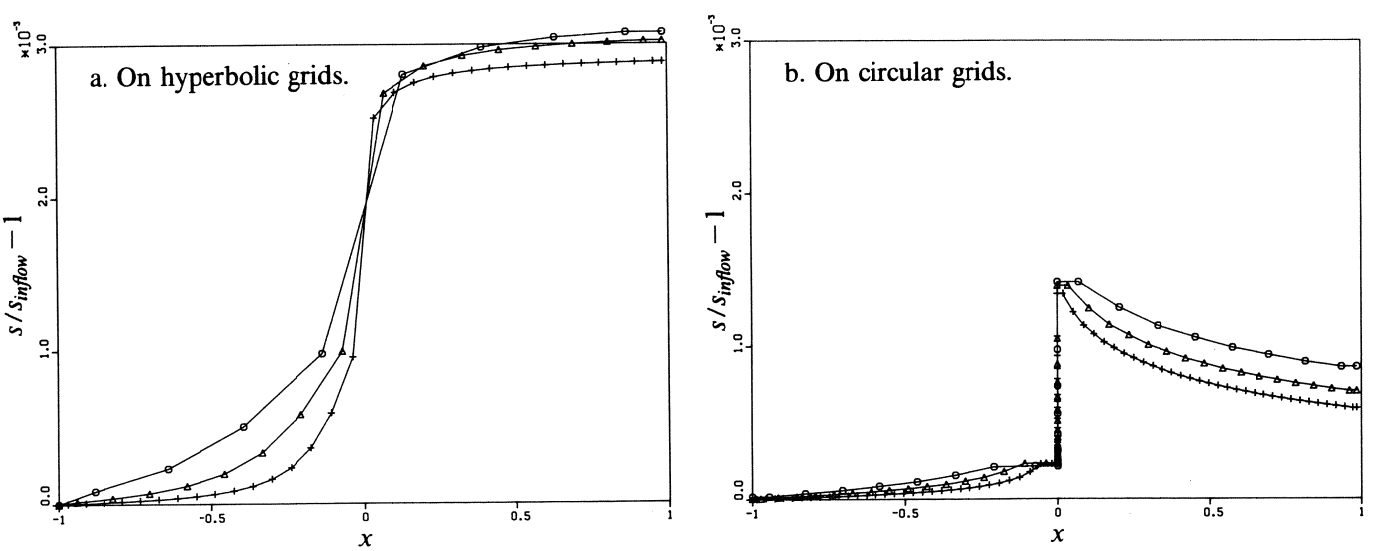

Figure 13. Entropy error along kinked wall, $\delta = 10°$,
○:8×8-grid, Δ:16×16-grid, +:32×32-grid.

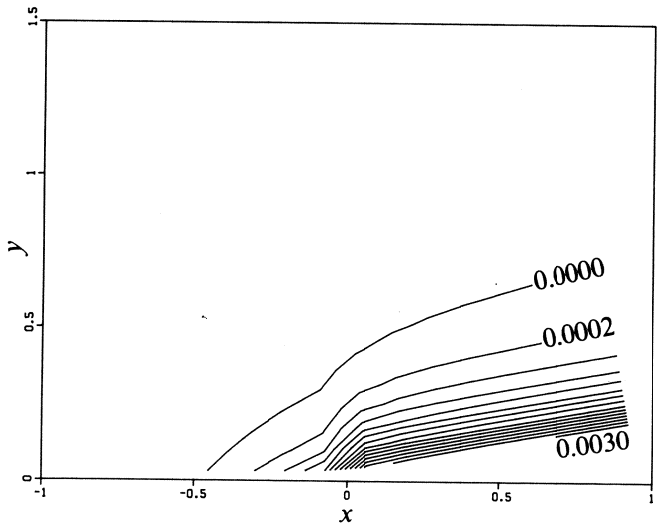

a. On 16×16-grid.

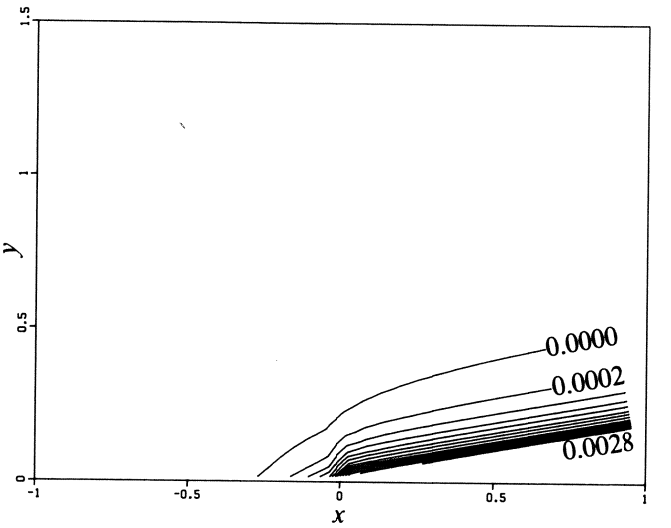

b. On 32×32-grid.

Figure 14. Iso-plots entropy error, hyperbolic grid, $\delta = 10°$.

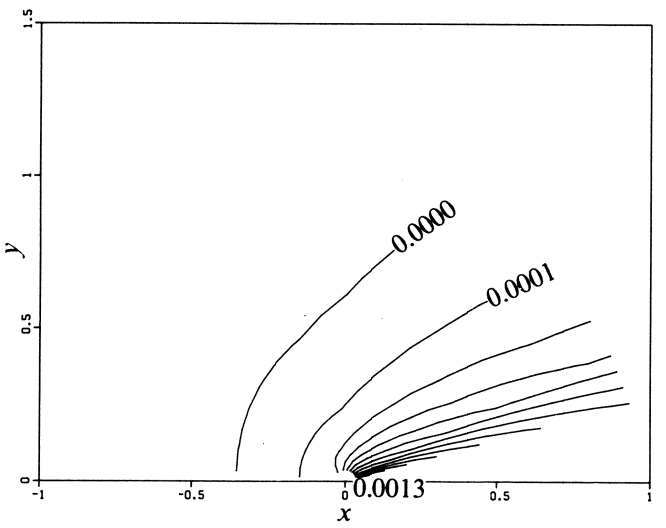

a. On 16×16-grid.

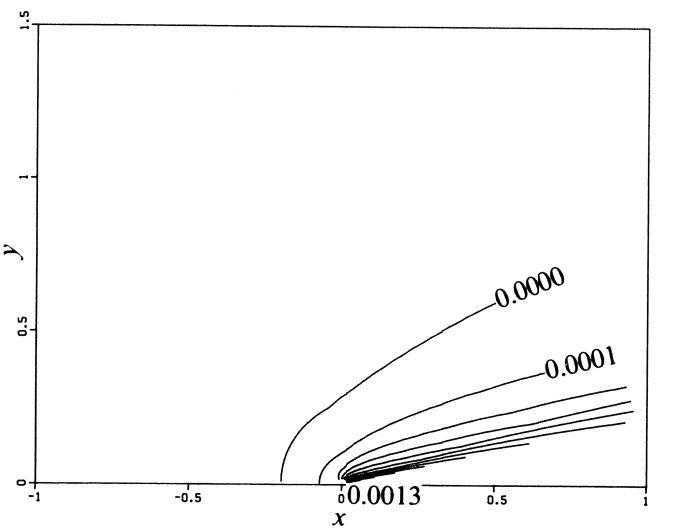

b. On 32×32-grid.

Figure 15. Iso-plots entropy-error, circular grid, $\delta = 10°$.

4. Singularity in the solution

In section 2.3 we found that the zeroth-order entropy error is probably not caused by the non-smoothness of the grid, in section 3.1 we found that the error is not caused by the implementation of the solid wall boundary condition, and in section 3.2 we found that it is also not caused by the use of a specific type of grid. In this section we will consider another possible (and now most likely) cause of the error: a singularity (i.e. a non-differentiability) in the (exact, continuous) solution at the kink.

4.1. Irrotational, incompressible flow

For the incompressible potential flow along a kinked wall, the exact solution of the continuous potential flow equation is known to be singular. In the polar r,θ-coordinates (Figure 16), for $\delta \leqslant \theta \leqslant \pi$, the velocity field is described by

$$\begin{aligned} u &= U r^{\frac{\delta}{\pi-\delta}} \cos(\theta - \frac{\theta-\delta}{\pi-\delta}\pi), \\ v &= U r^{\frac{\delta}{\pi-\delta}} \sin(\theta - \frac{\theta-\delta}{\pi-\delta}\pi), \end{aligned} \tag{22}$$

where U is a constant. For $0<\delta<\pi/2$, the velocity field clearly has a singularity at $r=0$. (There, it is not differentiable.)

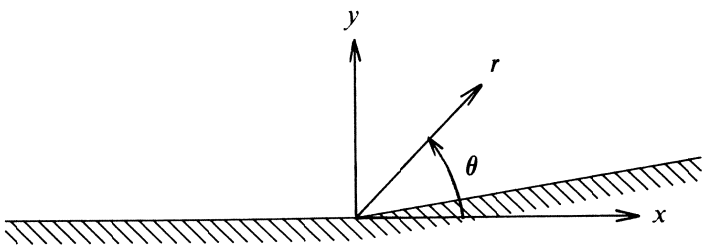

Figure 16. Polar coordinates at kink.

4.2. Incompressible potential flow with compressible Euler equations and source term

In this section, we investigate whether or not a singularity of the form r^α, $0<\alpha<1$, gives rise to errors which are similar to those found in the previous entropy distributions. We do this by approximating the incompressible potential flow field, by numerically solving the compressible Euler equations with proper source term. (Since the exact solution is known, we can easily compute each error component of the numerical solution.) The source term for the equations is found by substituting the exact, incompressible potential flow solution into the continuous compressible Euler equations. The incompressible potential flow solution satisfies the 'compressible-Euler-continuity' and '-momentum' equations, but the 'compressible-Euler-energy' equation is not satisfied. Therefore we (only) need a source term for the energy equation:

$$\frac{\partial(\rho u H)}{\partial x} + \frac{\partial(\rho v H)}{\partial y} = -\frac{1}{\gamma-1}\rho U^3 \frac{\delta}{\pi-\delta} r^{-\frac{\pi-4\delta}{\pi-\delta}} \cos(\frac{\theta-\delta}{\pi-\delta}\pi), \quad \delta \leqslant \theta \leqslant \pi. \tag{23}$$

In order not to let zeroth-order errors be introduced by the source term, we take $\delta=\pi/4$. For the computation we use the existing solution method applied to the first-order discretized Euler equations supplied with a first-order approximation of the source term.

In Figure 17, numerical results are presented as obtained on the hyperbolic grid. The results shown are the errors in the entropy-like function $z=\ln(p/\rho^{\gamma})$. (Notice that the function p/ρ^{γ} in the exact solution is not a constant.) The figure shows that at a distance from the wall the error is first-order accurate, but becomes zeroth-order accurate in the vicinity of the kink. From this we conclude that when the solution of the exact equations has a singularity at $r=0$, the numerical approximation to this solution has a zeroth-order error in the vicinity of $r=0$. In our numerical approximation of the subsonic compressible Euler flow along a kinked wall now, we have a zeroth-order error at the kink. So it is likely that the exact solution of the subsonic compressible Euler equations for the flow along a kinked wall, also has a singularity at the kink.

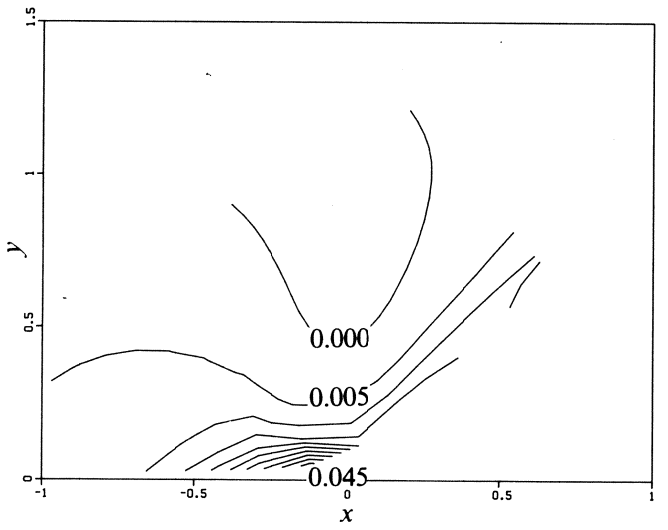

a. Iso-plot 'entropy' error, 16×16-grid.

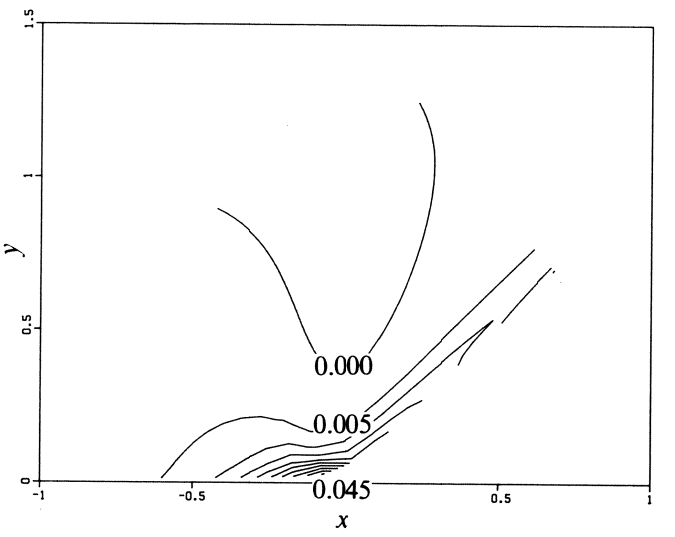

b. Iso-plot 'entropy' error, 32×32-grid.

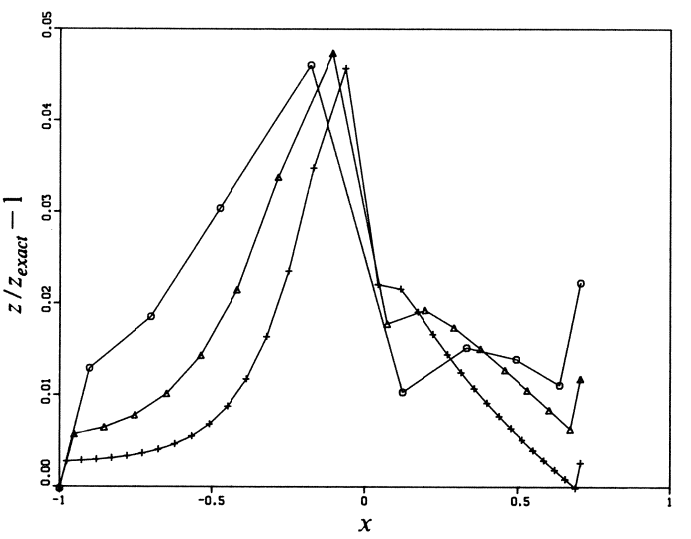

c. 'Entropy' error along wall,
O:8×8-grid, Δ:16×16-grid, +:32×32-grid.

Figure 17. 'Entropy' error ($z/z_{exact}-1$) potential flow solution, hyperbolic grid, $\delta=\pi/4$.

4.3. Transformation of variables and equations

In this section we investigate whether for compressible Euler flow, we can transform the dependent variables and the equations in such a way that only smooth (i.e. non-singular) functions remain to be approximated. Herewith we strive for a minor modification of the existing numerical method. We assume that the velocity field of the subsonic compressible Euler flow along a kinked wall has a singularity similar to that of the incompressible potential flow. In the previous sub-section it was suggested that if this is the correct form of the singularity, the approximate solution, obtained by solving the discretized Euler equations, should have a zeroth-order error behaviour. By extracting now such a singularity, we hope to remove this behaviour. Assume that u and v can be written as

$$\begin{aligned} u &= Ur^{\alpha}, \\ v &= Vr^{\alpha}, \end{aligned} \tag{24}$$

where U and V are smooth functions of x and y and where $\alpha=\delta/(\pi-\delta)$, $0<\delta<\pi/2$. (So U and V are singular at $r=0$.) Further, assume that the exact Euler flow is homentropic and isenthalpic. Then, along the wall we have for the speed of sound

$$c^2 = c_0^2 - \frac{\gamma-1}{2}(U^2+V^2)r^{2\alpha} = C_0^2 - C_1^2 r^{2\alpha}, \tag{25}$$

with C_0 a constant and C_1 a smooth function. If we assume that the enthalpy changes smoothly from one streamline to another, then (25) is valid everywhere in the flow field, with - in that case - both C_0 and C_1 a smooth function of x and y. Furthermore, C_1 is a known function of U and V. With $s=p/\rho^{\gamma}$ constant, we find for the density

$$\rho = (\gamma s)^{\frac{-1}{\gamma-1}} (C_0^2 - C_1^2 r^{2\alpha})^{\frac{1}{\gamma-1}} = (R_0 - R_1 r^{2\alpha})^{\frac{1}{\gamma-1}}, \tag{26}$$

and for the pressure

$$p = (\gamma^{\gamma} s)^{\frac{-1}{\gamma-1}} (C_0^2 - C_1^2 r^{2\alpha})^{\frac{\gamma}{\gamma-1}} = (P_0 - P_1 r^{2\alpha})^{\frac{\gamma}{\gamma-1}}. \tag{27}$$

In here, R_0, R_1, P_0 and P_1 are smooth functions of x and y, and R_1 and P_1 are known functions of U and V. Next we can transform the Euler equations (1)-(2) into equations to be satisfied by our new, smooth variables U, V, R_0, P_0. Substitution of (24)-(27) into e.g. $\mathbf{f(q)}$ as given in (2), yields

$$\mathbf{f(q)} = \begin{bmatrix} \rho u \\ \rho u^2 + p \\ \rho uv \\ \rho uH \end{bmatrix} = \begin{bmatrix} U\left[R_0 r^{\alpha(\gamma-1)} - R_1 r^{\alpha(\gamma+1)}\right]^{\frac{1}{\gamma-1}} \\ U^2\left[R_0 r^{2\alpha(\gamma-1)} - R_1 r^{2\alpha\gamma}\right]^{\frac{1}{\gamma-1}} + \left[P_0 - P_1 r^{2\alpha}\right]^{\frac{\gamma}{\gamma-1}} \\ UV\left[R_0 r^{2\alpha(\gamma-1)} - R_1 r^{2\alpha\gamma}\right]^{\frac{1}{\gamma-1}} \\ Us\frac{\gamma}{\gamma-1}\left[R_0^2 r^{\alpha(\gamma-1)} - R_0 R_1 r^{\alpha(\gamma+1)}\right]^{\frac{1}{\gamma-1}} \end{bmatrix}. \tag{28}$$

The transformed fluxes are complicated, non-linear functions of the dependent variables U, V, R_0 and P_0. The corresponding system of discretized equations cannot be solved by the existing method nor by a slightly modified version of it. Apart from the fact that the transformed equations require an ambitious modification of the existing numerical method, it is not yet certain whether or not the assumptions made on the singularity are correct. Therefore, we refrain from a further investigation of the transformed equations.

5. Getting round the entropy error by properly rounding the kink

In section 3.1 we computed the Euler flow along a continuously curved wall. There, the length l of the continuously curved wall segment (Figure 9) was the same for all three grids considered. In this section we re-compute the flow along a continuously curved wall as given by (21), but now we let l depend on the mesh size: $l=O(h^{\lambda})$, $\lambda>0$. For finite λ, it is clear that for $h\to 0$ the wall becomes kinked. The results of section 1.4 and 3.1 can be considered as those for the limit cases $\lambda=\infty$ and $\lambda=0$, respectively. (For $\lambda=\infty$, for all h, the continuously curved wall segment is reduced to a single point and the entropy error is zeroth-order.) The number of cells N lying along the curved part of the wall is $N=l/h$. Hence, with $l=O(h^{\lambda})$ we have $N=O(h^{\lambda-1})$. So for $\lambda<1$, N increases with decreasing h and for $\lambda>1$, N decreases. In the latter case, for $h\to 0$ we find that at the kink (which is in fact the curved part of the wall), there is only one mesh line. In that case we would have the same situation as for $\lambda=\infty$, the situation with zeroth-order entropy error. So, in order to have decreasing entropy errors for decreasing mesh size, we must take $\lambda<1$.

In Figure 18 now, we show the behaviour of the entropy error when l is decreased as a function of h. Herewith, for l we take $l=c_1h^{\lambda}$, c_1 constant, and for the maximum norm of the entropy error we assume the form $\|s/s_{inflow}-1\|=c_2h^{\mu}$, c_2 constant. Based on numerical experiments with $c_1=1$, μ has been determined for different values of λ, using a 16×16-, a 32×32- and a 64×64-grid. As expected, for $\lambda=0$ we find that $\mu\to 1$ for $h\to 0$. The main message of Figure 18 is that the flow along a continuously curved wall can be used indeed, to approximate the flow along a kinked wall. For any $\lambda\in(0,1)$, in the limit $h\to 0$, the curved wall becomes kinked and the error vanishes, because for any λ in that range it appears that $\|s/s_{inflow}-1\|=O(h^{\mu})$, $\mu>0$. (If we want to let the entropy error disappear at the same rate as l, then from Figure 18 we find that we should take $\lambda\approx 0.4$.)

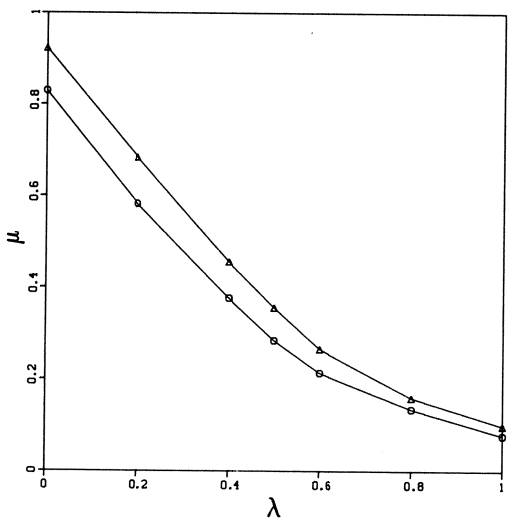

Figure 18. Order behaviour maximal entropy error, $\delta=10°$, properly rounded kink,
○:16×16-grid/32×32-grid, Δ:32×32-grid/64×64-grid.

6. Conclusions

In this paper we studied two possible causes of zeroth-order entropy errors, as encountered in the numerical approximation of subsonic Euler flow along a kinked wall: (i) non-smoothness of the grid and (ii) non-smoothness of the exact solution of the continuous Euler equations. (The approximation of the flow along a smooth wall shows, as expected, that the entropy error is not caused by the discretization of the solid wall boundary condition.)

Concerning the non-smoothness of the grid, it appears that the upwind finite volume discretization of the equations has a zeroth-order local discretization error at the kink in the grid. For supersonic flow this discretization error can be removed by simply extending the stencil of the discretization in the direction in which the grid is shifted. For subsonic flow a zeroth-order error remains. However, the numerical computation of a subsonic, non-uniform, parallel flow on a kinked grid *without* wall, suggests that the zeroth-order behaviour of the local discretization error does not cause the zeroth-order entropy error.

Concerning the non-smoothness (i.e. the being singular) of the exact solution, it is well-known that the incompressible potential flow along a kinked wall has a singularity at the kink. It is most likely that a similar singularity is adopted by the Euler flow. The numerical approximation of the incompressible potential flow, by means of the Euler equations with proper source term, shows that zeroth-order errors in the solution arise at the same places as in the approximation of the Euler flow. Extraction of a singularity from the dependent variables of the Euler equations, a singularity which is similar to that of the incompressible potential flow solution, does not lead to a set of equations which can be solved with the existing method.

Removing the zeroth-order error behaviour is not impossible. We find the paradoxical result that by making a less accurate (but specific) discretization of the geometry, a numerical solution with better error behaviour can be obtained. The less accurate discretization of the geometry employs smooth discrete versions of the exact kinked geometry. The flow along a smooth wall is used to *approximate* the flow along a kinked wall. By making the length of the curved part of the smooth wall dependent of the mesh size h, an $O(h^{\mu})$-entropy error, $\mu>0$, still can be obtained.

Acknowledgement

The authors wish to thank P.W. Hemker and P. Wesseling for their constructive comments.

References

1. P.W. Hemker and S.P. Spekreijse, 'Multiple grid and Osher's scheme for the efficient solution of the steady Euler equations', *Appl. Numer. Math.*, **2**, 475-493 (1986).
2. A. Dervieux, B. van Leer, J. Périaux and A. Rizzi (eds.), *Proc. GAMM-Workshop on the Numerical Simulation of Compressible Euler Flows,* Rocquencourt, 1986; *Notes on Numerical Fluid Dynamics, Vol. 26,* Vieweg, Braunschweig, 1989.
3. P.D. Lax, 'Hyperbolic systems of conservation laws II', *Comm. Pure Appl. Math.*, **10**, 537-566 (1957).
4. S. Osher and F. Solomon, 'Upwind difference schemes for hyperbolic systems of conservation laws', *Math. Comput.*, **38**, 339-374 (1982).
5. B. Koren, 'Euler flow solutions for transonic shock wave - boundary layer interaction', *Int. J. Numer. Methods in Fluids,* **9**, 59-73 (1989).
6. B. Koren, 'Defect correction and multigrid for an efficient and accurate computation of airfoil flows', *J. Comput. Phys.*, **77**, 183-206 (1988).